Experimental and Theoretical Studies of VOC Adsorption on Acid-Activated Bentonite in a Fixed-Bed Adsorber

Abdelfattah Amari,*,† Mohamed Chlendi,† Abdelaziz Gannouni,† and Ahmed Bellagi‡

Department of Chemical Engineering, National School of Engineering, Gabes 6029, Tunisia, and Department of Energy Engineering, National School of Engineering, Monastir 5019, Tunisia

In this work, the adsorption of toluene onto acid-activated bentonite in a fixed bed using an inverse gas chromatography was investigated. Adsorbent was prepared according to an optimized activation process. Experimental and theoretical studies were established to evaluate the removal efficiency of toluene by adsorption on acid-activated bentonite and to predict kinetics parameters. A suitable adsorption model has been developed to simulate the measured data based on linear driving force approximation. The fourth-order Runge−Kutta method was used to integrate the partial differential equations, and the resulting functions were simultaneously solved to obtain the breakthrough profiles. Theoretical predictions from the model were compared with column adsorption data to ensure the validity of the model. Adequate agreement between simulations and experimental data was reached.

1. Introduction

Recently, emissions of volatile organic compounds (VOCs) have become one of the most stringent environmental challenges in many industrial chemical plants such as coating, spray painting, dyeing, and polymer processing. Because of their high vapor pressure, VOCs can easily evaporate into the atmosphere and be considered as one of the major contributors to air pollution by the formation of photochemical ozone and secondary organic aerosol (SOA).[1−3] Controlling VOCs emission is a major concern of the industries commitment in regard to environmental issues.[4] There are many different techniques available to VOCs reduction and control, particularly adsorption, which is a reliable chemical engineering method widely used thanks to the flexibility of the system, the low energy, and the cheap operation costs.[5−7] VOCs are removed from the bulk gas by physical adsorption onto the surface adsorbent.

Activated carbon is a very useful adsorbent for VOCs control due to its developed microporosity, which ensures good adsorption capacities.[8] However, some disadvantages may limit its application such as the sensibility to high temperature, the difficulty in regenerating high-boiling point solvents, the flammability, and humidity control requirement.[9] Hence, different alternative adsorbents need to be developed to overcome these problems. In fact, the primary requirement of an adsorbent is the selectivity, which determines the preferential adsorption of one or more components and the chemical and physical stability under various operating conditions. As an alternative to activated carbon, high silica zeolites and bentonite have several advantages. Particularly, the use of bentonite is attracting more and more attention due to its resistance to high thermal operations and its adsorption affinity for VOCs.[10] In its natural state, bentonite has limited adsorption ability. To improve its adsorptive properties and to produce homogeneous and well-defined materials for use as adsorbents and catalysts, different treatments of bentonite, most frequently by inorganic acids, have been studied.[11−13] Acid-activation of bentonite can improve its behavior by removing impurities and various exchangeable cations from the structure. The important physical changes are the increase of the external specific surface area and the average pore volume.[14−16] Acid-activated bentonite becomes an important and widely used class of mesoporous solids for industrial applications.[12−15] This material with large pore distribution and good mechanical stability has shown a high affinity for VOC.[17] In bed operation, adsorbate is initially transferred from the bulk gas through an external film to the external surface of the particle. After that, molecules of the adsorbate, which diffuse into the particle, are adsorbed on active sites and then diffuse along the surface. Film transfer and pore diffusion are treated as sequential steps, but pore diffusion and surface diffusion generally take place together. Numerous models have been published in recent years to describe the process of fixed bed adsorption.[18] Simplified models are often obtained by using appropriate approximations to get substantial savings in computational time. However, every approximate solution has its own restricted scope of validity, which should be accurately defined; otherwise wrong results might be obtained owing to significant deviations from the exact solution.[19,20]

For column adsorption studies, the most commonly used adsorption models include the linear driving force (LDF)[21−23] thanks to its simplicity and accuracy in reproducing the adsorption of organic molecules on different materials, both organic and inorganic.[24] It is one of several simplified versions of the transport dispersion model. This model considers that the mass transfer resistance in the solid phase is a dominant mass transfer effect.

The LDF model is an approximation to the solution of Fickian diffusion inside a spherical particle. This expression assumes that the mass transfer rate of adsorption is proportional to the difference between the equilibrium concentration and the gas phase concentration of the component.

Many works had used the LDF model to determine the adsorption and desorption breakthrough behaviors of volatile organic compounds (VOC) on activated carbons and zeolites.[23−25] They concluded that the experimental adsorption and desorption curves could be predicted fairly well by the LDF model. The previous successful application of the LDF model to VOC adsorption and desorption on activated carbons and zeolites has led us to use it in the present study to predict the breakthrough curves of VOC adsorption onto acid-activated bentonite. The

* To whom correspondence should be addressed. Tel: +21698660059. Fax: +21675221704. E-mail: abdelfattah.amari@enig.rnu.tn.
† Department of Chemical Engineering.
‡ Department of Energy Engineering.

10.1021/ie100296n
Published on Web 10/12/2010

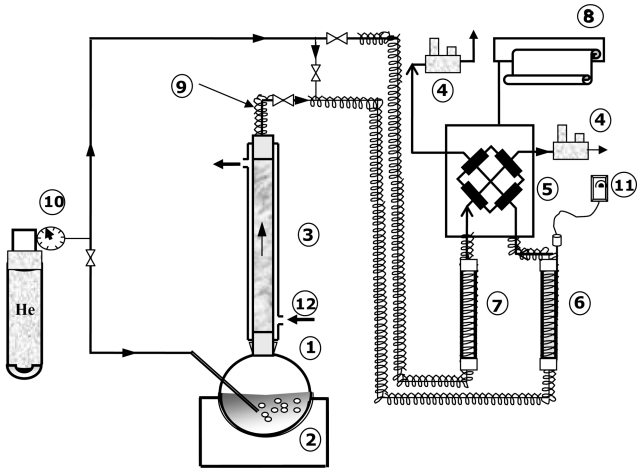

1. solvent evaporator
2. Heat of solvent evaporator
3. Condenser
4. Mass flow controller
5. Gas chromatograph
6. Fixed bed (Adsorption column)
7. column of Reference
8. chart recorder
9. thermal ribbon
10. Pressure indicator
11. temperature controller
12. Refrigerating water circulator

Figure 1. Experimental setup used for the adsorption of VOCs on acid-activated bentonite in a fixed bed column.

accuracy of the predictions is assessed by comparing them with toluene experimental breakthrough curves.

In this study, adsorption of toluene onto acid-activated bentonite in fixed bed was carried out using an inverse gas chromatography. Toluene was chosen as a model compound based on the fact that it was detected in many industrial sites and it is considered as one of the most often reported indoor VOCs.

2. Experimental Section

2.1. Material. Acid-activated bentonite employed as the adsorbent in the present study was prepared by acid attack (H_2SO_4) on raw bentonite. This activated bentonite is the result of an optimized activation process of bentonite for toluene adsorption using central composite orthogonal design (CCOD). Activation process and optimization of experimental conditions were detailed in our previous work.[17] Temperature, contact time, liquid/solid mass ratio, and acid concentration were chosen as process variables for the optimization of toluene adsorption. These optimal conditions, obtained for the preparation of acid-activated bentonite, were the following: a temperature of 96.2 °C, a contact time of 6.93 h, a liquid/solid ratio of 5.98, and an acid concentration of 32.94%. Using the adsorption of nitrogen at −196 °C, the textural properties for activated bentonite were determined by an automatic sorption analyzer (Quantachrome Autosorb AS1C). Acid-activated bentonite has a BET specific surface area of 195 m^2/g, a pore volume of about 0.46 cm^3/g, and a most frequent pore size of 62 Å. Prior to the experiments, the adsorbent was kept in a drying vacuum oven at 130 °C for more than 24 h to remove impurities and possible water vapor.

2.2. Adsorption Dynamics. A fixed bed adsorption unit given in Figure 1 was examined to study adsorption dynamics of toluene in a column packed with acid-activated bentonite. The bed was about 20 cm long and an inner radius of 0.9 cm and was packed to 9 cm height with acid-activated bentonite. The bulk density of adsorbent was 437 kg/m^3, and the bed void fraction was about 0.126. Before packing, the adsorbent was dried in a vacuum oven. To support the adsorbent and uniform gas distribution, two knit meshes were placed at the top and the bottom of the bed, ensuring in this way a uniform flow throughout the adsorption bed. A thermocouple was installed at middle of the bed to monitor the temperature of the bed.

The carrier gas was helium with a purity of 99.9%. The sorbent used as the stationary phase in the column was conditioned before use for at least 2 h under a stream of the carrier gas. In this unit, helium gas was divided into two lines. One was for pure helium gas as a carrier, and the other was connected into the solvent evaporator. To ensure homogeneous mixing of solvent vapors with pure helium gas stream, a static in-line mixer was installed at the inlet section of the adsorption column (not represented in Figure 1).

The gas concentration of VOCs was adjusted by controlling the flow rate of carrier gas. During adsorption, the concentration at the exit of the adsorption bed was monitored by a gas chromatograph (IGC 10M) fitted with a thermal conductivity detector. Before starting each experiment, the temperature of the saturator should be maintained constant to generate a constant VOCs partial pressure by circulating through the outlet the gas stream of the saturator. When the required concentration was reached and kept stable, the gas stream was driven through the adsorbent tubes to start the breakthrough process. The carrier gas flow rate was measured by a Teflon Flowmeter (AALBORG. Monsey, NY). Because of the long retention times in the column and the risk of obtaining disqualified chromatographic peaks at low temperature, the column and line temperature should be higher than the temperature of sorbate-saturated pressure to avoid any gas condensation. After reaching saturation of the adsorbent bed, the adsorbed VOC was desorbed using nitrogen gas at a flow rate of 70 mL/min.

Our experiments may encounter some possible sources of errors and uncertainties in the measurement of breakthrough curves. These sources of errors can result from the following: (i) The change in temperature, which can influence the carrier gas flow rate controlled by mass flowmeters. This may introduce small errors on the input pressure of VOCs estimated at about 2.5%. (ii) The temperature measured in the column may be somewhat different from that of the adsorbent. These tiny errors in this case are hard to calculate. Before conducting the experiments, a sufficient large period of time was used, so that the temperature can be considered as constant. (iii) The effects of buoyancy can lead to changes in the density of the mixture VOC/He that increases with temperature at constant pressure. This error in our work area is not considered significant; it is less or about 1%. All these errors just mentioned are disregarded.

3. Mathematical Model

The system considered here is an isothermal adsorption column packed with porous adsorbent. The adsorption column was subjected to axial dispersion, external film mass transfer resistance, and solid diffusion resistance. The following assumptions were made in the analysis: (i) No chemical reactions occur in the column. (ii) Pressure, temperature, carrier gas flow rate, and feed concentration are assumed to be constant and controlled within 3−5%. (iii) The gas phase is assumed to obey the ideal gas behavior. (iv) Radial temperature, concentration, and velocity gradient within the bed are neglected. (v) Accumulation of carrier gas in the pores of the solid phase is disregarded. (vi) The LDF model was applied for presenting the adsorption dynamics in column.

On the basis of the above assumptions, the mass balance for a fixed-bed column with axial dispersion can be described for one-dimensional axial flow by the following equation

$$-D_{ax}\frac{\partial^2 C}{\partial z^2} + u\frac{\partial C}{\partial z} + \frac{\partial C}{\partial t} + \frac{(1-\varepsilon)}{\varepsilon}\rho_p\frac{\partial q}{\partial t} = 0 \quad (1)$$

where C is the gas phase concentration of VOC, t is the time, z is the axial coordinate, D_{ax} is the axial dispersion coefficient, ρ_p is the density of the particle of activated bentonite, u is the gas velocity through the interstices of the packed bed, ε is the bed void fraction, and q is the adsorption capacity (Abbreviations).

In this study, it is assumed that a local equilibrium is attained at the fluid−solid interface and that the equilibrium can be described by the Freundlich isotherm. The validity of this model for the representation of the toluene equilibrium data was discussed in a previous work.[26] The adsorption isotherms were satisfactorily fitted with the Freundlich model in the low range pressure (0−30 kPa)

$$q = \alpha P^{\beta} \quad (2)$$

where α and β are the parameters of the Freundlich model that were determined by extrapolation from data of adsorption isotherms measured in the temperature range 120−182 °C.

The appropriate initial and boundary conditions can be written as follows

$$C = C_0, \text{ for } z = 0 \text{ and } t > 0 \quad (3)$$

$$\frac{\partial C}{\partial z} = 0, \text{ for } z = L \text{ and } t > 0 \quad (4)$$

where C_0 is an initial gas concentration in fluid (kg/m^3). q_0 is the initial adsorbed phase concentration (kg/kg).

Generally assuming a plug flow without axial dispersion that is in any section perpendicular to fluid flow, velocity and concentration are uniform. As reported by Ragavan and Ruthven,[27] this assumption is justified if the ratio between the length of the column, L, and the mean particle diameter, dp, is greater than 20.

In our case, L/dp = 480. Thus the axial dispersion can be neglected.

Equation 1 becomes

$$u\frac{\partial C}{\partial z} + \frac{\partial C}{\partial t} + \frac{(1-\varepsilon)}{\varepsilon}\rho_p\frac{\partial q}{\partial t} = 0 \quad (5)$$

This is a partial differential equation in two variables. To eliminate the influence of the space variable, the column is assumed to be a cascade of n-series identical units with a constant volume for each one equal to v. Let v (m^3) be the gas volume in each unit

$$v = \frac{V}{n} = \frac{sL}{n} \quad (6)$$

The physicochemical conditions within each unit are identical. Villermaux[28] shows that the number of constant volume units in a fixed bed can be expressed as

$$n = \frac{Pe_{ax}}{2} + 1 \quad (7)$$

where Pe_{ax} is an axial Peclet number.

Taking into account the term of accumulation, eq 5 can be written as follow

$$Q(C_0 - C) = \varepsilon V\frac{dC}{dt} + \rho_b V(1-\varepsilon)\frac{dq}{dt} \quad (8)$$

The LDF model for gas adsorption kinetics is frequently and successfully used in predicting the adsorption of VOCs in fixed bed column. According to the LDF method, the reaction rate is governed by the difference between the temporal and the equilibrium adsorbed phase concentrations.[21] The mass transfer rate across the fluid film can be expressed by the following equation

$$\frac{dq}{dt} = k_{LDF}(q^* - q) \quad (9)$$

The mass balance for the first cell and the n^{th} cell is written by

Unit 1

$$Q(C_0 - C_1) = \varepsilon\frac{V}{n}\frac{dC_1}{dt} + \rho_b\frac{V}{n}(1-\varepsilon)\frac{dq_1}{dt} \quad (10)$$

$$\frac{dq_1}{dt} = k_{LDF}(q_1^* - q_1) \quad (11)$$

Unit n

$$Q(C_{n-1} - C_n) = \varepsilon\frac{V}{n}\frac{dC_n}{dt} + \rho_b\frac{V}{n}(1-\varepsilon)\frac{dq_n}{dt} \quad (12)$$

$$\frac{dq_n}{dt} = k_{LDF}(q_n^* - q_n) \quad (13)$$

By introducing the dimensionless coordinates, the preceding set of partial differential equations (PDEs) was written and the solution was numerically obtained.

$$X = \frac{C}{C_0} \quad \text{and} \quad Y = \frac{q}{q^*}\frac{C}{C_0} \quad (14)$$

$$q = \alpha C^{\beta}; \quad q_0^* = \alpha C_0^{\beta} \quad Y^* = \frac{q}{q_0^*} = \left(\frac{C}{C_0}\right)^{\beta} = X^{\beta} \quad (15)$$

For n^{th} unit

Unit 1

$$Q(1 - X_1) = \varepsilon v\frac{dX_1}{dt} + \rho_b v(1-\varepsilon)\frac{q^*(C_0)}{C_0}\frac{dY_1}{dt} \quad (16)$$

$$\frac{dY_1}{dt} = k_{LDF}(Y^*(X_1) - Y_1) \qquad Y^*(X) = X^{\beta} \quad (17)$$

Unit n

$$Q(X_{n-1} - X_n) = \varepsilon v\frac{dX_n}{dt} + \rho_b v(1-\varepsilon)\frac{q^*(C_0)}{C_0}\frac{dY_n}{dt} \quad (18)$$

$$\frac{dY_n}{dt} = k_{LDF}(Y^*(X_n) - Y_n) \qquad Y^*(X) = X^{\beta} \quad (19)$$

In this paper, a computer program based on the mathematical model described by eqs 18 and 19 with initial and boundary condition given by eqs 3 and 4 was developed. In this investigation, the mathematical model was transformed into a set of first order ordinary differential equations using the finite difference method. The calculations were performed in MATLAB of reference: 7.3.0.267 (R2006b).

k_{LDF} was determined by the best fitting of the experimental data to the mathematical model based on the minimization of the least-squares coefficient, according to $\delta = \sum(C_{exp} - C_{mod})^2$

4. Evaluation of Axial Dispersion Coefficient

Axial dispersion coefficient, D_{ax}, can be calculated using the Peclet number of grain (Pe_g) from the nondimensional relationship of Edwards and Richardson[29]

$$\frac{1}{\mathrm{Pe}_g} = \frac{0.73\varepsilon}{\mathrm{Re} \times \mathrm{Sc}} + \frac{0.5}{1 + \dfrac{9.49\varepsilon}{\mathrm{Re} \times \mathrm{Sc}}} \tag{20}$$

where Re and Sc are Reynolds number and Schimdt number defined below, respectively,

$$\mathrm{Re} = \frac{\rho_f u d_p}{\mu} \tag{21}$$

$$\mathrm{Sc} = \frac{\mu}{\rho_f D_m} \tag{22}$$

Equations 21 and 22 are applicable in the Reynolds number range and in the Schimdt number range of

$$0.008 < \mathrm{Re} < 400 \tag{23}$$

$$\text{and} \quad 0.28 < \mathrm{Sc} < 2.2 \tag{24}$$

D_m is the molecular diffusion coefficient of toluene in helium. It was estimated from the equation of Fuller et al.[30] as follows (Abbreviations):

$$D_m = \frac{10^{-3} T^{1.75}}{P\left(\left(\sum v_A\right)^{1/3} + \left(\sum v_B\right)^{1/3}\right)^2} \sqrt{\left(\frac{1}{M_A} + \frac{1}{M_B}\right)} \tag{25}$$

The axial Peclet number in the column is deduced from the Peclet number of grain by the relation

$$\mathrm{Pe}_{ax} = \mathrm{Pe}_g \frac{L}{d_p} \tag{26}$$

$$\text{Also} \quad \frac{1}{\mathrm{Pe}_g} = \frac{D_{ax}}{u d_p} \tag{27}$$

Combining eqs 20, 26 and 27, the axial dispersion coefficient can be given by the following equation

$$D_{ax} = 0.73\varepsilon D_m + \frac{0.5 u d_p}{1 + \dfrac{9.49\varepsilon D_m}{u d_p}} \tag{28}$$

5. Results and Discussions

5.1. Model Fitting of Breakthrough Curves for VOC Adsorption in a Fixed Bed. The simulations of the adsorption of toluene on acid-activated bentonite were performed using the mathematical model described in Section 3. The experimental data and simulated curves are presented in Figures 2 and 3, and the characteristics of the adsorption bed and the operating conditions are summarized in Table 1. The typical breakthrough curves give the evolution of the C/C_0 ratio as a function of time, where C is the concentration of toluene at the outlet of the adsorption bed, and C_0 is the concentration of toluene at the inlet.

The steep nature of these curves is indicative of an efficient use of the adsorbent in dynamic processes. In some cases, the simulations are good (experiments 1, 2, and 5 for example), both qualitatively and quantitatively. Experiments conducted in these conditions can be correctly reproduced by the simulations. However, in some other cases, good coherence between experiment and simulation is observed only up to a fraction of C/C_0 around 0.7; beyond this value, there is a gap at the top of the forehead, particularly in the breakthrough curves corresponding to experiments 3, 4, 6, and 7. The simulated curves are somewhat remote from the experience. The error is because the temperature was not practically stable in the column, a phenomenon that is difficult to reproduce by simulation.

Pentchev et al.[31] had indicated that it is difficult to obtain uniform temperature in column section in small diameter laboratory column as in our case (diameter $d = 1.8$ cm, length $L = 9$ cm) and relatively low superficial gas velocity ($v = 2 \times 10^{-3}$ to 4×10^{-3} m·s^{-1}). The thermal effect of adsorption leads to deformation of the temperature profiles along the column and this directly affects the total amount adsorbed in the bed and breakthrough at the exit.

In fact, since the adsorption is exothermic, the resistance to heat transfer also affects the mass transfer. Ruthven[32] found that the early stages of adsorption in isothermal column are very sensitive to any resistance to the transfer of the solute in the

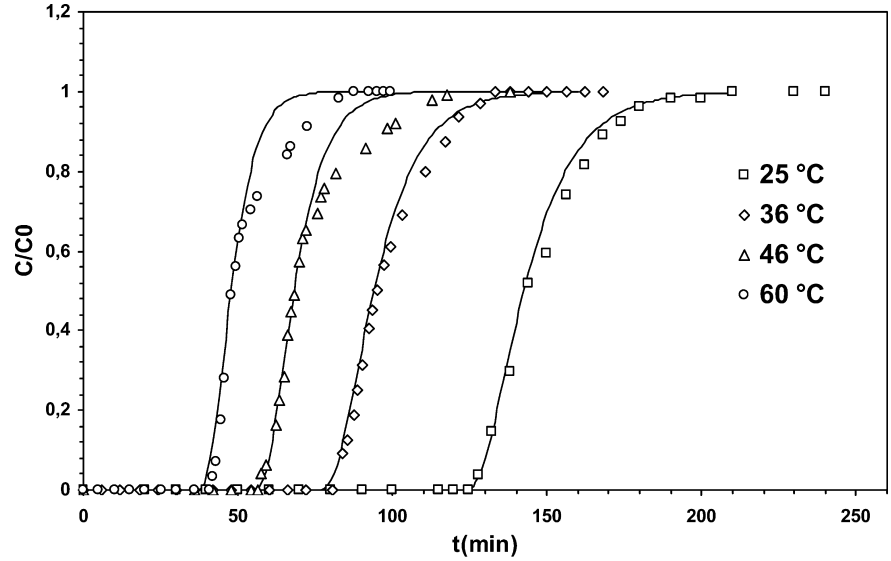

Figure 2. Experimental and predicted breakthrough curves of toluene adsorption onto acid-activated bentonite at different temperatures (experiments 1, 2, 3, and 4).

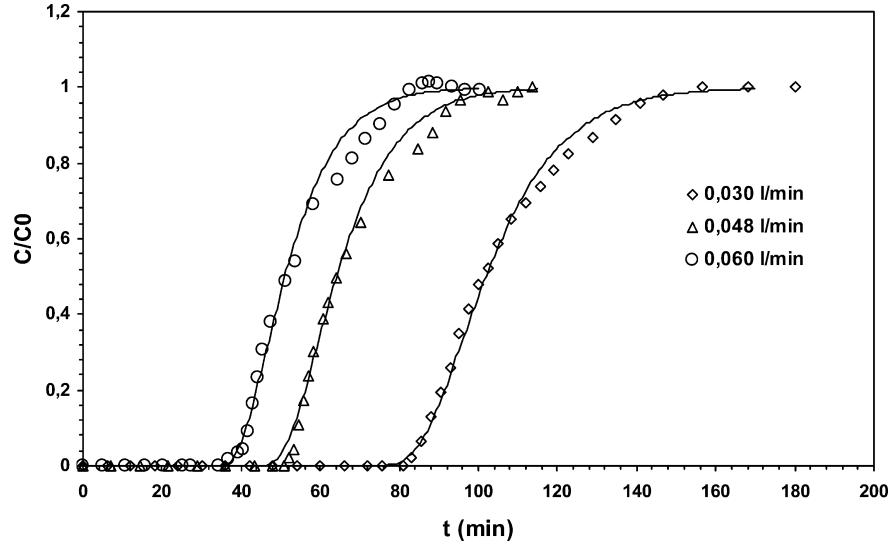

Figure 3. Experimental and predicted breakthrough curves of toluene adsorption onto acid-activated bentonite at different flow rates (Experiments 5, 6, and 7).

Table 1. Experimental Conditions and Simulated Parameters Used During the Adsorption of Toluene onto Acid-Activated Bentonite

parameters	notation	exp 1	exp 2	exp 3	exp 4	exp 5	exp 6	exp 7
temperature (°C)	T	25	36	46	60	46	46	46
total volume of flow gas (L/min)	Q	5.12×10^{-2}	5.66×10^{-2}	5.88×10^{-2}	5.66×10^{-2}	3.05×10^{-2}	4.80×10^{-2}	6.0×10^{-2}
bed inlet concentration (kg/m^3)	C_0	11.60×10^{-2}	11.60×10^{-2}	11.60×10^{-2}	11.60×10^{-2}	22.44×10^{-2}	22.44×10^{-2}	22.44×10^{-2}
dynamic viscosity of the mixture (Pa•s)	μ	13.88×10^{-6}	14.25×10^{-6}	14.57×10^{-6}	1.502×10^{-6}	13.69×10^{-6}	13.69×10^{-6}	13.69×10^{-6}
density of gas mixture (kg/m^3)	ρ_f	27.70×10^{-2}	26.79×10^{-2}	25.90×10^{-2}	24.80×10^{-2}	36.90×10^{-2}	36.9×10^{-2}	36.9×10^{-2}
mean particle diameter (μm)	d_p	187.50	187.50	187.50	187.50	187.50	187.50	187.50
molecular diffusion coefficient of toluene in helium (m^2/s)	D_m	2.87×10^{-5}	3.06×10^{-5}	3.24×10^{-5}	3.49×10^{-5}	32.38×10^{-6}	32.38×10^{-6}	32.38×10^{-6}
Reynolds number	Re	13.02×10^{-3}	13.07×10^{-3}	12.91×10^{-3}	11.51×10^{-3}	10.09×10^{-3}	15.88×10^{-3}	19.86×10^{-3}
Schmidt number	Sc	173.97×10^{-2}	173.80×10^{-2}	173.45×10^{-2}	173.11×10^{-2}	114.68×10^{-2}	114.68×10^{-2}	114.68×10^{-2}
Peclet number	Pe	117.93	118.24	116.58	103.79	60.37	94.92	118.55
number of cells	n	60	61	60	53	32	49	61

macropores, while at the end, it is the thermal effects of adsorption that are responsible for the diffusion kinetics.

On the other hand, Bart et al.[33] had reported that for practical use the influence of adsorption heat on the adsorption process is negligible at low concentrations. For this reason, when modeling the adsorption of organic substances, the usual assumption is to neglect the influence of the heat of adsorption.[33,34] It was also shown that the beginning of breakthough curve coincides with the maximum elevation of temperature, and then, the temperature decreases to reach its initial value.

5.2. The Effect of Temperature. The effect of temperature in the range 25−60 °C on the breakthrough curve for the same gas flow rate and concentration ($C_0 = 11.6 \times 10^{-2}$ kg/m^3) is shown in Figure 2. The results indicated that the breakthrough curves were steeper at high temperature than at low temperature due to the increasing micropore and macropore diffusion with temperature. The adsorption is an exothermic process ($\Delta H < 0$); at high temperatures, the adsorption capacity relatively decreased to small equilibrium constants and an earlier breakthrough curve would occur (Table 2).

5.3. The Effect of Feed Flow Rate. Flow rate is also one of the important parameters in determining the efficiency of adsorbents in continuous treatment process of COV effluents at pilot or industrial scales. This is because the accumulation of toluene in fixed bed column is largely dependent on the quantity of sorbent inside the column. Figure 3 shows the sorption breakthrough curves obtained by varying the flow rate from 30 to 60 mL/min for a fixed temperature of 46 °C and a constant initial toluene concentration ($C_0 = 22.44 \times 10^{-2}$ kg/m^3).

Table 2. Values of Maximum Adsorption Capacities Obtained by Measure of Breakthrough Curves and Calculated by the Model of Freundlich

	maximum adsorption capacity (mg/g)		
experiments	measured	calculated	error (%)
1	93.369	98.896	5.920
2	64.287	72.522	12.809
3	51.970	54.658	5.174
4	34.768	36.628	5.350
5	74.602	82.162	10.134
6	77.553	82.162	5.943
7	80.784	82.162	1.706

As expected, both the breakthrough curves and saturation time are influenced by the gas flow rate. By reducing the flow rate, the breakthrough and exhaustion time increased. This means that the volume of VOC that can be treated is effectively increased and a longer time is required for reaching the column saturation. This gas flow rate dependency can be accounted for by the fact that for lower values of flow rate, the interaction between the component and the sorbent is greater. However, for higher flow rates an earlier breakthrough curve would occur. This is because higher flow rates can make greater linear driving force between gas phase and solid phase.[35,36]

Even more than the visual comparison of breakthrough curves, the measured adsorption capacity and that calculated by the model of Freundlich were determined. Table 2 summarizes the values of adsorption capacities for all experiments. A quite good agreement with an average error of 6.71% is observed between experimental and calculated data. The adsorption capacity decreased with increasing temperature (experiments

Table 3. Estimated Values of Model Parameters

experiments	T (°C)	k_{LDF} (s^{-1})	k_a ($m \cdot s^{-1}$)	D_{ax} ($m^2 \cdot s^{-1}$)	D_e ($m^2 \cdot s^{-1}$)
1	25	2.67×10^{-3}	1.11×10^{-7}	2.65×10^{-6}	1.56×10^{-12}
2	36	3.50×10^{-3}	1.46×10^{-7}	2.82×10^{-6}	2.05×10^{-12}
3	46	6.00×10^{-3}	2.50×10^{-7}	2.98×10^{-6}	3.51×10^{-12}
4	60	11.67×10^{-3}	4.86×10^{-7}	3.22×10^{-6}	6.84×10^{-12}
5	46	3.67×10^{-3}	1.53×10^{-7}	2.98×10^{-6}	2.15×10^{-12}
6	46	4.00×10^{-3}	1.67×10^{-7}	2.98×10^{-6}	2.34×10^{-12}
7	46	4.25×10^{-3}	1.77×10^{-7}	2.98×10^{-6}	2.49×10^{-12}

1, 2, 3, and 4) because the toluene adsorption onto activated bentonite can be considered as physical adsorption, and the adsorption capacity decreases with increasing temperature.

The small discrepancy (i.e., less than 7% on average) between the experimental and the predicted values of adsorption capacity, as shown in Table 2, might be a result of the assumptions made to solve the fixed bed model, in addition to those of the kinetic and equilibrium models. Nonetheless, considering all the potential sources of errors, the level of accuracy observed, is a strong indication that the proposed models provide an acceptable representation of the behavior of toluene adsorption in a fixed bed column containing acid-activated bentonite.

5.4. Estimated Parameters of the Model Used in Simulation. By optimizing the numerical breakthrough curves with the experimental data, the values of the overall mass transfer coefficients (k_a) were determined from eq 29

$$k_{LDF} = k_a a_p \tag{29}$$

a_p is the specific area referred to the unit volume of bed (m^2/m^3) given and calculated by

$$a_p = \frac{6(1-\varepsilon)}{d_p} \tag{30}$$

k_{LDF} was determined by fitting the experimental data with the mathematical model by using a computer program specifically developed for this purpose. The numerical method used was a finite difference method with a forward finite difference explicit scheme. Equations 18 and 19 were simultaneously solved taking into account the initial conditions. Different k_{LDF} values were supposed and the computer program was run obtaining a theoretical breaktrough curve. Then, the experimental and theoretical data were compared and the correlation coefficient was calculated. Once the optimum k_{LDF} value was reached, the only unknown variable in eq 31 is D_e. Its value largely depends on the surface properties of the adsorbent

$$k_{LDF} = \frac{15 D_e}{r_p^2} \tag{31}$$

Results on external mass transfer coefficient, overall mass transfer coefficient, axial dispersion coefficient, and effective diffusion coefficient obtained at different conditions are given in Table 3. These results show that no significant effect of the flow rate (experiments 5, 6, and 7) on all the kinetic coefficients is observed. This can be interpreted by the fact that such parameters are only related to the proprieties of adsorbent. Furthermore, it is well-known that the increase in flow rate decrease the mass transport resistance across the external gas film.[37]

It is also observed that the adjusted parameter k_{LDF} and the effective diffusion coefficient, D_e, increase significantly with temperature (experiments 1, 2, 3, and 4). This investigation is obvious since for microporous adsorbents, such as bentonite in our case, the diffusion process is represented by activation law and the effect of temperature is usually expressed by the Arrhenius law.[38] Compared to k_{LDF}, k_a, and D_e, the axial dispersion coefficient, D_{ax}, has a negligible impact on the model performance. The values of D_{ax} remained almost unchanged. This is expected as the simulated breakthrough curves at various D_{ax} (not shown) were almost the same.

6. Conclusion

In this study, the linear driving force (LDF) model for gas adsorption kinetics was successfully used for analysis of toluene adsorption column dynamic data. The model was capable of describing the uptake of toluene in the temperature range of 25−60 °C with a standard deviation of less than 6% in majority cases. The shape of the breakthrough curves as predicted by the model was in close agreement with the experimental data.

The effect of temperature and the gas flow rate on the adsorption of toluene was experimentally investigated. Under high reaction temperatures, the model-predicted data indicate that the adsorption constant rate increases whereas equilibrium adsorption capacities decrease. The adsorption process is an exothermic process; high temperature will decrease the adsorption capacity.

Abbreviations

a_p = outer surface area of grain per unit bed volume, m^2/m^3
C = gas-phase concentration in bulk flow, kg/m^3
C^* = equilibrium concentration of the adsorbate, kg/m^3
C_0 = bed inlet concentration, kg/m^3
D_m = molecule diffusivity, $m^2 \cdot s^{-1}$
D_{ax} = axial dispersion coefficient, $m^2 \cdot s^{-1}$
D_e = effective diffusivity coefficient, $m^2 \cdot s^{-1}$
d_p = mean particle diameter, m
k_a = overall mass transfer coefficient
k_{LDF} = mass transfer coefficient through gas film
Q = total volume of flow gas, $m^3 \cdot min^{-1}$
q = amount of gas adsorbed, g/g
q^* = equilibrium amount adsorbed, g/g
q_0^* = equilibrium amount adsorbed at C_0, g/g
L = length of the fixed bed column, m
Pe_{ax} = axial Peclet number, dimensionless
Pe_g = Peclet number of grain, dimensionless
Re = Reynolds number, dimensionless
r_p = particle radius, m
s = section of column, m^2
Sc = Schmidt number, dimensionless
M = molecular weight, g/mol
P = pressure, Pa
T = temperature, °C
t = time, s
u = interstitial velocity, cm/s
v = volume of cell
V = total volume of column, m^3
X = dimensionless parameter in equation
Y = dimensionless parameter in equation
z = axial distance, cm

Greek Symbols

α, β = Freundlich model parameters
ε = bed void fraction
μ = dynamic viscosity of the mixture, Pa·s
v_A = molecular volume of toluene, $cm^3\ g^{-1}\ mol^{-1}$
v_B = molecular volume of helium, $cm^3\ g^{-1}\ mol^{-1}$
ρ_f = gas density, kg/m^3
ρ_b = bulk density, kg/m3
ρ_p = particle density, kg/m3

Superscript/Subscript

0 = inlet
n = 1, 2, 3, ...
p = particle
g = grain
ax = axial
exp = experimental
mod = model

Literature Cited

(1) Forstner, H. J. L.; Flagan, R. C.; Seinfeld, J. H. Secondary Organic Aerosol from the Photooxidation of Aromatic Hydrocarbons: Molecular Composition. *Environ. Sci. Technol.* **1997**, *31*, 1345–1358.

(2) Carter, W. P. L.; Cocker, D. R., III; Fitz, D. R.; Malkina, I. L.; Bumiller, K.; Sauer, C. G.; Pisano, J. T.; Bufalino, C.; Song, C. A. New Environmental Chamber for Evaluation of Gas-phase Chemical Mechanisms and Secondary Aerosol Formation. *Atmos. Environ.* **2005**, *39*, 7768–7788.

(3) Seinfeld, J. H.; Pandis, S. N. *Atmospheric Chemistry and Physics: from Air Pollution to Climate Change*, 2nd ed.; J. Wiley: Hoboken, NJ, 2006.

(4) Khan, F. I.; Ghoshal, A. K. Removal of Volatile Organic Compounds from Polluted Air. *J. Loss Prev. Process Ind.* **2000**, *13*, 527–545.

(5) Hu, X.; Qiao, S.; Zhao, X.; Lu, G. Adsorption Study of Benzene in Ink-bottle-like MCM-41. *Ind. Eng. Chem. Res.* **2001**, *40*, 862–867.

(6) Serrano, D. P.; Calleja, G.; Botas, J. A.; Gutierrez, F. J. Adsorption and Hydrophobic Properties of Mesostructured MCM-41 and SBA-15 Materials for Volatile Organic Compound Removal. *Ind. Eng. Chem. Res.* **2004**, *43*, 7010–7018.

(7) Guillemot, M.; Mijoin, J.; Mignard., S.; Magnoux, P. Adsorption of Tetrachloroethylene on Cationic X and Y Zeolites: Influence of Cation Nature and of Water Vapor. *Ind. Eng. Chem. Res.* **2007**, *46*, 4614–4620.

(8) Manjare, S. D.; Ghoshal, A. K. Studies on Adsorption of Ethyl Acetate Vapor on Activated Carbon. *Ind. Eng. Chem. Res.* **2006**, *45*, 6563–6569.

(9) Blocki, S. W. Hydrophobic Zeolite Adsorbent: A Proven Advancement in Solvent Separation Technology. *Environ. Prog.* **1993**, *12*, 226–230.

(10) Morrissey, F. A.; Grismer, M. E. Kinetics of Volatile Organic Compound Sorption/Desorption on Clay Minerals. *J. Contam. Hydrol.* **1999**, *36*, 291–312.

(11) Fijal, J.; Klapyta, Z.; Zietkiewicz, J.; Zyla, M. On the Mechanism of the Montmorillonite Acid Activation, I. Degradation of Ca-Montmorillonite Structure. *Mineral. Pol.* **1975**, *6*, 29–41.

(12) Gannouni, A.; Bellagi, A.; Baganne, M. Preparation of Activated Clay for the Bleaching of Olive Oil. Ann. *Chim. Sci. Mat.* **1999**, *24*, 407–416.

(13) Komadel, P.; Madejova, J. Acid Activation of Clay Minerals. In *Handbook of Clay Science*; Bergaya, F., Theng, B. K. G., Lagaly, G., Eds; Elsevier: Amsterdam, 2006; Vol. 1, pp 263−287.

(14) Kheok, S. C.; Lim, E. E. Mechanism of Palm Oil Bleaching by Montmorillonites Clay Activated at Various Acid Concentrations. *J. Am. Oil Chem. Soc.* **1982**, *59*, 129–131.

(15) Morgan, D. A.; Shaw, D. B.; Sidebottom, M. J.; Soon, T. C.; Taylor, R. S. The Function of Bleaching Earths in the Processing of Palm, Palm Kernel and Coconut Oils. *J. Am. Oil Chem. Soc.* **1985**, *62*, 292–299.

(16) Taylor, D. R.; Jenkins, D. B.; Ungermann, C. B. Bleaching with Alternative Layered Minerals: A Comparison with Acid Activated Montmorillonite for Bleaching Soybean oil. *J. Am. Oil Chem. Soc.* **1989**, *66*, 334–341.

(17) Amari, A.; Gannouni, A.; Chlendi, M.; Bellagi, A. Optimization by Response Surface Methodology (RSM) for Toluene Adsorption on to Prepared Acid Activated Clay. *Can. J. Chem. Eng.* **2008**, *86*, 1093–1102.

(18) Wang, C. H.; Hwang, B. J. A General Adsorption Isotherm Considering Multi-Layer Adsorption and Heterogeneity of Adsorbent. *Chem. Eng. Sci.* **2000**, *55*, 4311–4321.

(19) Yang, R. T.; Doong, S. J. Gas Separation by Pressure Swing Adsorption: a Pore Diffusion Model for Bulk Separation. *AIChE J.* **1985**, *31*, 1829–1842.

(20) Chahbani, M. H.; Tonder, D. Mass Transfer Kinetics in Pressure Swing Adsorption. *Sep. Purif. Technol.* **2000**, *20*, 185–96.

(21) Gkueckauf, E. Theory of Chromatography. Part 10. Formulas for Diffusion into Spheres and their Application to Chromatography. *Trans. Faraday Soc.* **1955**, *51*, 1540–1551.

(22) Crittenden, J. C.; Weber, W. J. Predictive Model for Design of Fixed-bed Adsorbers: Single-Component Model Verification. *J. Environ. Eng.* **1978**, *104*, 433–443.

(23) Malek, A.; Farooq, S. Kinetics of Hydrocarbon Adsorption on Activated Carbon and Silica gel. *AIChE J.* **1997**, *43*, 761–776.

(24) Brosillon, S.; Manero, M. H.; Foussard, J. N. Mass Transfer in VOC Adsorption on Zeolite: Experimental and Theoretical Breakthrough Curves. *Environ. Sci. Technol.* **2001**, *35*, 3571–3575.

(25) Patton, A.; Crittenden, B. D.; Perera, S. P. Use of the Linear Driving Force Approximation to Guide the Design of Monolithic Adsorbents. *Chem. Eng. Res. Des.* **2004**, *82*, 999–1009.

(26) Amari, A.; Chlendi, M.; Gannouni, A.; Bellagi, A. Optimised Activation of Bentonite for Toluene Adsorption. *Appl. Clay Sci.* **2010**, *47*, 457–461.

(27) Ragavan, N. S.; Ruthven, D. M. Numerical Simulation of a Fixed Bed Adsorption Column by the method of Orthogonal Collocation. *AIChE J.* **1983**, *29*, 922–925.

(28) Villermaux, J. *Génie de la réaction chimique conception et fonctionnement des réacteurs*, Technique et documentation; Lavoisier: Paris, 1982.

(29) Edwards, M. F.; Richardson, J. F. Gas Dispersion in Packed Beds. *Chem. Eng. Sci.* **1968**, *2*, 109–121.

(30) Fuller, E. N.; Schettler, P. D.; Giddings, J. C. A New Method for Prediction of Binary Gas-phase Diffusion Coefficients. *Ind. Eng. Chem.* **1966**, *58*, 19–27.

(31) Pentchev, I.; Paev, K.; Seikova, I. Dynamics of non Isothermal Adsorption in Packed Bed of Biporous Zeolites. *Chem. Eng. J.* **2002**, *85*, 245–257.

(32) Ruthven, D. M. *Principles of adsorption and adsorption processes*; Wiley Intersciences: New York, 1984.

(33) Bart, H. J.; Germerdonk, R.; Ning, P. Two-Dimensional non-Isothermal Model for Toluene Adsorption in a Fixed-bed adsorber. *Chem. Eng. Process.* **1996**, *35*, 57–64.

(34) Vortmeyer, D.; Michael, K. The Effect of Non-uniform Flow Distribution on Concentration Profiles and Breakthrougt Curves of Fixed Bed Adsorbers. *Chem. Eng. Sci.* **1985**, *40*, 2135–2138.

(35) Petrovic, L. J.; Thodos, G. Mass Transfer in the Flow of Gases Through Packed Beds - Low Reynolds Number Region. *Ind. Eng. Chem. Fundam.* **1968**, *7*, 274–280.

(36) Yun, J. H.; Choi, D. K.; Kim, S. H. Equilibria and Dynamics for Mixed Vapors of BTX in an Activated Carbon Bed. *AIChE J.* **1999**, *45*, 751–760.

(37) Lv, L.; Zhang, Y.; Wang, K.; Ray, A. K.; Zhao, X. S. Modeling of the Adsorption Breakthrough Behaviors of Pb^{2+} in a Fixed Bed of ETS-10 Adsorbent. *J. Colloid Interface Sci.* **2008**, *325*, 57–63.

(38) Barrer, R. M. *Zeolites and clay minerals as sorbents and molecular sieves*; Academic Press: London, 1978.

Received for review February 6, 2010
Revised manuscript received September 5, 2010
Accepted October 1, 2010

IE100296N